



Contents lists available at ScienceDirect

Nuclear Instruments and Methods in Physics Research A

journal homepage: www.elsevier.com/locate/nima

Signal encoding method for a time-of-flight PET detector using a silicon photomultiplier array

Sun Il Kwon^{a,c,d}, Jae Sung Lee^{a,b,c,d,*}^a Department of Nuclear Medicine, Seoul National University, Seoul 110-744, Republic of Korea^b Department of Biomedical Sciences, Seoul National University, Seoul 110-744, Republic of Korea^c Interdisciplinary Program in Radiation Applied Life Science, Seoul National University, Seoul 110-744, Republic of Korea^d Institute of Radiation Medicine, Medical Research Center, Seoul National University, Seoul 110-744, Republic of Korea

ARTICLE INFO

Article history:

Received 21 January 2014

Received in revised form

8 May 2014

Accepted 12 May 2014

Available online 20 May 2014

Keywords:

Silicon photomultiplier (SiPM)

Positron emission tomography (PET)

Time-of-flight (TOF)

ABSTRACT

The silicon photomultiplier (SiPM) is a promising photosensor for magnetic resonance (MR) compatible time-of-flight (TOF) positron emission tomography (PET) scanners. The compact size of the SiPM allows direct one-to-one coupling between the scintillation crystal and the photosensor, yielding better timing and energy resolutions than the light sharing methods that have to be used in photomultiplier tube (PMT) PET systems. However, the one-to-one coupling scheme requires a huge volume of readout and processing electronics if no electric signal multiplexing or encoding scheme is properly applied. In this paper, we develop an electric signal encoding scheme for SiPM array based TOF PET detector blocks with the aim of reducing the complexity and volume of the signal readout and processing electronics. In an $M \times N$ SiPM array, the output signal of each channel in the SiPM array is divided into two signal lines. These output lines are then tied together in row and column lines. The row and column signals are used to measure the energy and timing information (or vice versa) of each incident gamma-ray event, respectively. Each SiPM channel was directly coupled to a $3 \times 3 \times 20 \text{ mm}^3$ LGSO crystal. The reference detector, which was used to measure timing, consisted of an R9800 PMT and a $4 \times 4 \times 10 \text{ mm}^3$ LYSO crystal and had a single time resolution of $\sim 200 \text{ ps}$ (FWHM). Leading edge discriminators were used to determine coincident events. Dedicated front-end electronics were developed, and the timing and energy resolutions of SiPM arrays with different array sizes (4×4 , 8×8 , and 12×12) were compared. Breakdown voltage of each SiPM channel was measured using energy spectra within various bias voltages. Coincidence events were measured using a ^{22}Na point source. The average coincidence time resolution of 4×4 , 8×8 , and 12×12 SiPM arrays were 316 ps, 320 ps, and 335 ps (FWHM), respectively. The energy resolution of 4×4 , 8×8 , and 12×12 SiPM arrays were 11.8%, 12.5%, and 12.8% (FWHM), respectively. Because of length differences between each SiPM channel and summed signal output on printed a circuit board, propagation delay of $\sim 111 \text{ ps}$ was observed. A signal encoding method for a TOF PET block detector using SiPMs has been developed to reduce the complexity and volume of the signal readout and processing electronics required. The proposed method showed promising results, which were measured for various SiPM array sizes.

© 2014 Elsevier B.V. All rights reserved.

1. Introduction

Positron emission tomography (PET) is one of the most important medical imaging modalities for the visualization of the functional and molecular information of pathologic structures in the living body. The combination of PET with X-ray computed tomography (CT) enables the incorporation of more accurate anatomical information for the interpretation and analysis of PET

data. Another recent advance in PET devices is the time-of-flight (TOF) information measurement capability [1,2]. The TOF information on mutually annihilated photons is useful for improving the reconstructed PET image quality, reducing the radiation dose, and/or shortening the scan time [3–5]. Gap artifact reduction in partial ring PET systems is another example of the benefits that we can derive from TOF measurements [6–8].

The photomultiplier tube (PMT) is the photosensor that is used in current commercially available TOF PET scanners. Efforts to improve the timing properties of the PMT are continuing (i.e. enhanced quantum efficiency in the photoelectric conversion process and reduced transit time spread in the electron transport). Promising results have been reported from recent studies

* Correspondence to: Department of Nuclear Medicine, Seoul National University College of Medicine, 28 Yungun-Dong, Chongno-Gu, Seoul 110-744, Republic of Korea. Tel.: +822 2072 2938; fax: +822 745 2938.

E-mail address: jaes@snu.ac.kr (J.S. Lee).

performed with these advanced PMTs [9–11]. However, PMTs have several well-known drawbacks, including their sensitivity to magnetic fields and their size, which is much larger than the individual pixelated scintillation crystals used in current PET systems.

Meanwhile, the silicon photomultiplier (SiPM) is a promising semiconductor photosensor for future use in both TOF PET/CT and PET/magnetic resonance imaging (MRI) scanners because the SiPM is insensitive to magnetic fields and has internal gain and timing properties that are compatible with the PMT [12,13]. It also has a compact size that enables direct one-to-one coupling between the scintillation crystal and the photosensor, yielding better timing and energy resolutions than the light sharing methods that are currently used in PMT PET systems. Recently, many encouraging studies showed the feasibility of using the SiPM for PET and the initial promising reconstructed images using SiPM PET scanners [14–19]. The excellent timing resolution of SiPM-based PET detectors reported recently in the literature also warrants the realization of MR-compatible TOF PET scanners with better timing resolution than the current level [20–22].

Although one-to-one coupling between the scintillation crystal and the SiPM has the advantages mentioned above, this method requires a huge volume of readout and processing electronics if no electrical signal multiplexing or encoding scheme is properly applied. Therefore, in this study, we utilized a projection-based electric signal encoding scheme for SiPM array based TOF PET detector blocks; with this scheme, we can reduce the complexity and volume of the signal readout and processing electronics. We also evaluated the effects of the SiPM array size on the timing and energy resolutions of the proposed detector block, because the combination of the multiple SiPM channels results in a higher dark count rate that has potential adverse effects on the physical performance.

2. Materials and methods

2.1. Projection-based signal encoding method

In an $M \times N$ SiPM array, the output signal of each SiPM channel is directly coupled to the pixelated scintillation crystal and is divided into two signal lines [Fig. 1]. These output lines are tied together in row and column lines [23]. These row and column signals are used to measure the energy and timing information (or vice versa) of each incident gamma-ray event, respectively. The 2D position of the gamma-ray interaction is determined by a combination of row and column signals. By applying this method, the number of output channels is reduced from $M \times N$ to $M + N$. The easy extensibility of this method with its flexible array size provides another advantage.

Each of the row and column signal lines would then be connected to an amplifier stage. Amplifier stages with different characteristics that are suitable for either energy or timing measurement would be preferred [21]. Simple inverting or non-inverting amplifiers and complex multi-stage amplifiers, such as differentiators and high-order shaping filters, can all be used in the amplifier stages.

However, it must be noted that a too large array size and too high encoding ratio can lead to degradation of the timing and energy resolutions and the count rate performance because of the increased dark count rate, resistance–capacitance (RC) value, signal pass length difference, and dead time loss. Therefore, careful evaluation of the performances of the detector blocks with different array sizes is necessary to balance the signal encoding ratio and the detector performance.

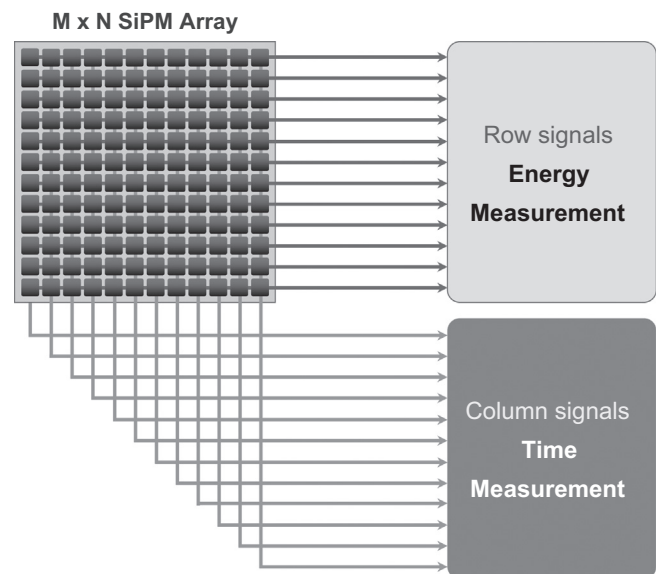


Fig. 1. Conceptual diagram of the projection-based signal encoding method. Output signals from the SiPM channels are tied together in row and column lines. The row and column signals are used to measure the energy and timing information of each incident gamma-ray event.

2.2. Front-end electronics and crystal block for concept verification

To implement the projection-based signal encoding method, anode signal from a SiPM channel was split into two signals through a resistor (47Ω) and tied together in each row and column directions as shown in [Fig. 2(a)]. A decoupling capacitor of $0.1 \mu\text{F}$ was used at each SiPM anode output. Front-end printed circuit board developed for testing the signal encoding method is shown in [Fig. 2(b)]. For concept verification, 4×4 channel SiPM devices (MPPC S11064-050P, Hamamatsu Photonics K.K., Japan) [18,19,24] were used to assemble an up to 12×12 SiPM array. Each SiPM channel has an active area of $3 \times 3 \text{ mm}^2$, consisting of 3600 pixels with a size of $50 \times 50 \mu\text{m}^2$. Each of the row and column signals was amplified using a high speed and high bandwidth amplifier with a simple inverting scheme. The gain of the column amplifiers ($\times 10$) was set to be higher than that of the row amplifiers ($\times 4$) for improved timing performance [20,21]. The output signal of each amplifier was connected with a LEMO cable connector. To avoid the influence of uneven path lengths during PCB trace routing, trace paths between each SiPM anode output and each row/column amplifier were made symmetric. In addition, each row or column trace path from an output of each amplifier to each LEMO cable connector had the same length. Careful impedance matching was done during PCB design.

While all the SiPM cathodes were connected to a common high voltage supply, each SiPM anode was connected to each of the output channels of the digital-to-analog (DAC) converter (octal, 16 bit, buffered voltage output type). The magnitude of the DAC output was controlled by using dedicated software via an I²C (inter-integrated circuit) interface to provide different bias voltage levels that are optimized for each SiPM. To reduce the complexity of circuits due to bias connections, one SiPM device (4×4 SiPM array) was supplied by one bias voltage [Fig. 2(a)].

The scintillation crystal that we have used throughout this study is the lutetium gadolinium oxyorthosilicate (LGSO) crystal ($\text{Lu}_{1.9}\text{Gd}_{0.1}\text{SiO}_4$: Ce; Hitachi Chemical Co., Ltd.) [25,26]. Each SiPM channel was directly coupled to a $3 \times 3 \times 20 \text{ mm}^3$ LGSO crystal, which was wrapped with a 3 M-enhanced spectral reflector (ESR) polymer with a thickness of 0.065 mm . Optical grease (Saint-Gobain BC-630, refractive index of 1.465) was used to optically

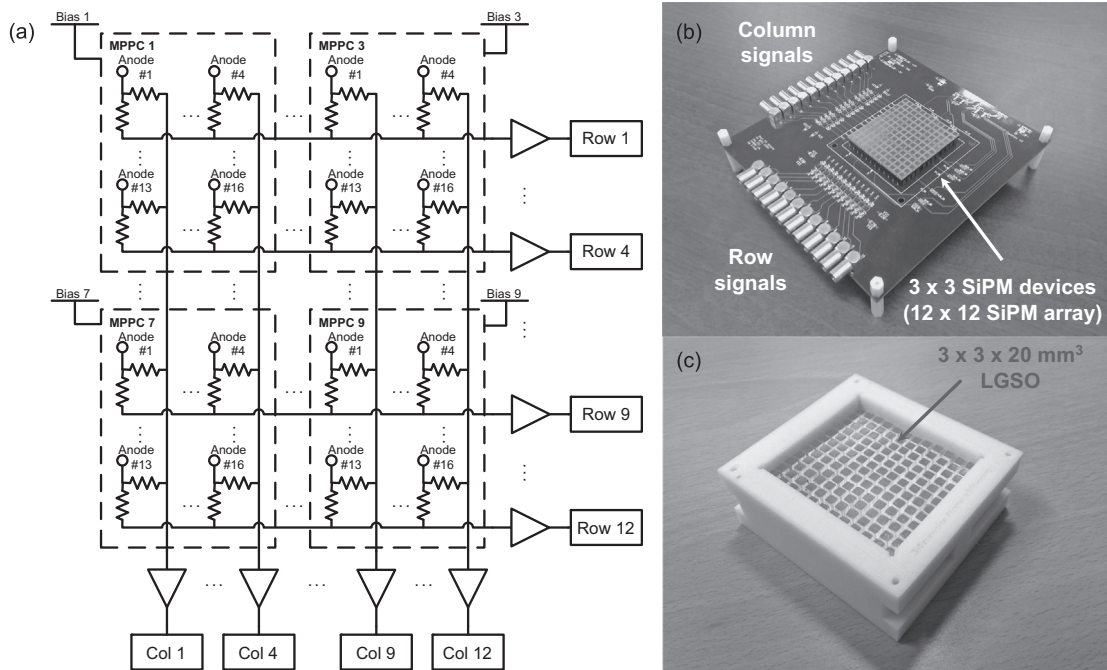


Fig. 2. Front-end electronics circuit implemented for testing of the projection-based signal encoding method (a), PCB board (b), and the LGSO crystal array (c).

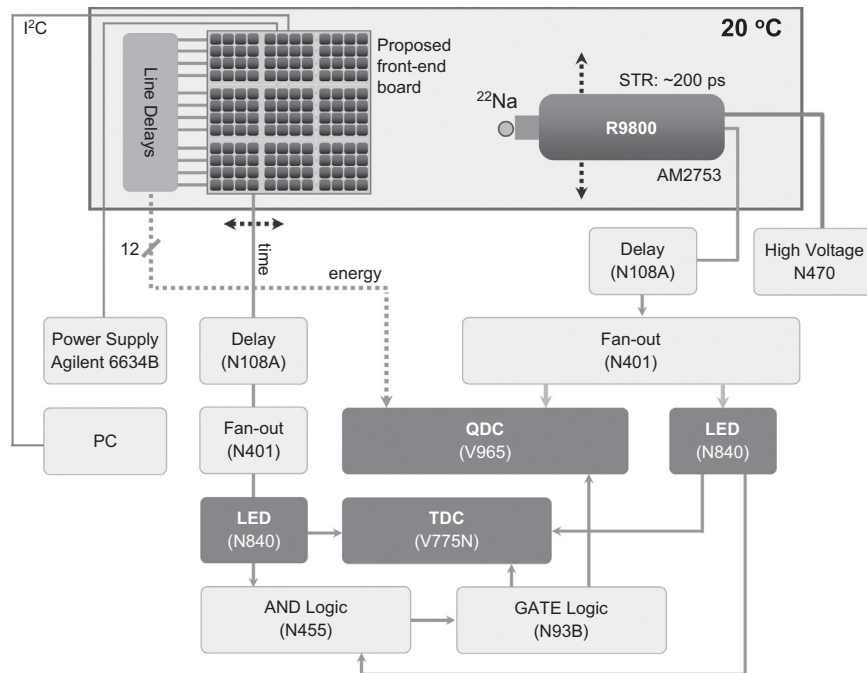


Fig. 3. Test setup for performance measurement of the developed detector block and the signal encoding method.

couple the crystal to the SiPM. To match the pitch of the crystal array with that of the SiPM array (the vertical and horizontal pitches were 4.50 mm and 4.05 mm, respectively), the crystal array was assembled using an acrylonitrile butadiene styrene (ABS) frame constructed with a 3D printer (Mojo, Stratasys, USA). Fig. 2(c) shows the 12 × 12 LGSO crystals held by the ABS frame.

2.3. Measurement setup

Fig. 3 shows the test setup for performance measurement of the developed detector block with its front-end electronics using a ²²Na

point source (diameter < 0.3 mm). A reference detector was used to detect the coincidental gamma-ray events only. The reference detector consisted of an R9800 fast PMT (Hamamatsu Photonics K.K.) and a 4 × 4 × 10 mm³ LYSO crystal, which was wrapped with a 3 M-ESR polymer [11]. The reference detector has a single time resolution of ~200 ps, which was measured with a bias voltage of 1300 V and a threshold level of ~3% (percentage from average peak voltages for 511 keV) in a leading edge discriminator (LED). A ²²Na point source was attached on the reference detector. The distance between ²²Na point source and the developed detector was ~30 cm. During the measurement, the reference detector and point source were moved in parallel with the surface of SiPM.

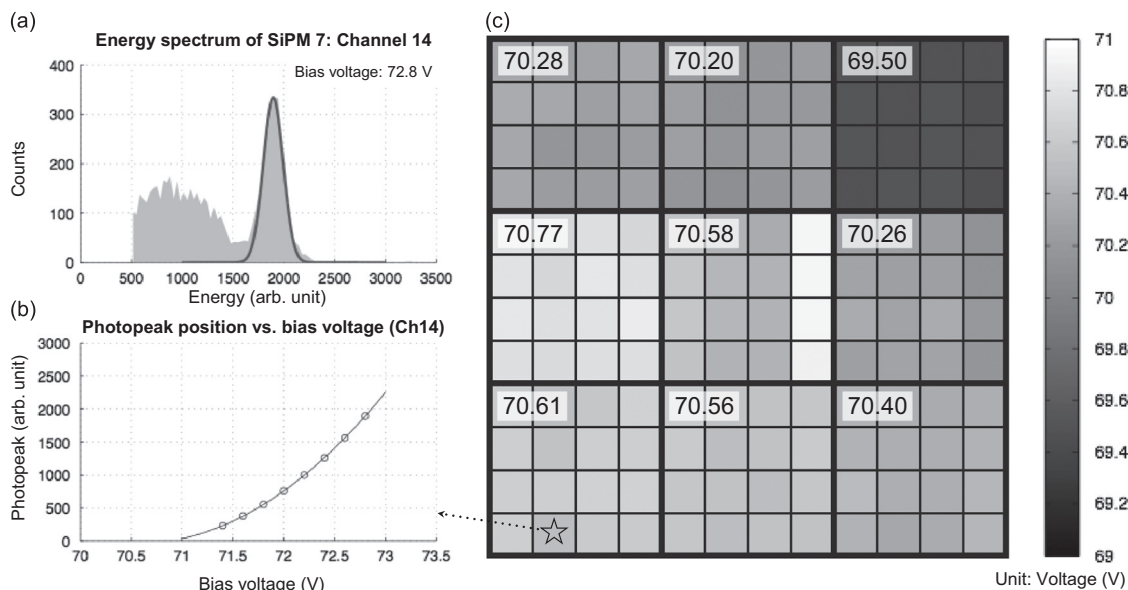


Fig. 4. Energy spectrum (a) and photopeak position as a function of bias voltage (b) of a SiPM channel (SiPM 7: channel 14 indicated by star mark). (c) Breakdown voltage distribution of each channel in all 12×12 SiPM arrays. The SiPM channels in each of the SiPM devices (packaged by a solid line) showed uniform breakdown voltage distributions. Each average bias voltage of one SiPM device (4×4) was noted on the top-left corner.

Because the properties of the SiPM output depend on the operating temperature [12,13], the developed and reference detectors were placed in a temperature-controlled box with a constant temperature of 20 °C. All output signals from the two detectors emerged from the box through a small hole (diameter: 5 cm). To discriminate between the signals and the noise from each detector, LED NIMs (nuclear instrument modules, N840, CAEN, Italy) were used. The LED output pulses were used to determine coincidence events and to obtain the timing information of the incident gamma-rays. The coincidence events were determined by using an AND NIM module (N455, CAEN), and the output pulses of the AND module generated gate pulses using a gate module (N93B, CAEN). These gate pulses were then used to integrate the input pulses from each of the detectors for energy measurement in a charge-to-digital converter (QDC) VME module (V965, CAEN). The gate pulses were also used as common-stop pulses in a time-to-digital converter (TDC) VME module (V775N, CAEN) to measure the time information of the coincidence signals. The TDC module measures time differences of up to 140 ns with 35 ps/bit resolution. The output pulses from the LED were used as start signals for the TDC. Appropriate cable lengths were added to the QDC inputs to ensure that the SiPM signals arrive within the gate pulses. To measure energy information from each row signal, all rows were connected into a 16-channel QDC. Because the AND logic had only two signal inputs, output of the reference detector and a selected column of developed detector block were connected into the inputs of an AND logic. Data from all SiPM channels were acquired while changing the column lines.

2.4. Experiments

The breakdown voltages of all the SiPM channels were estimated at first, because most of the properties of the SiPM output are related to the breakdown voltage [12,20]. The timing resolution of the SiPM detector was then measured under different bias voltages and trigger threshold levels to find the optimal bias voltage for each SiPM. The timing and energy performances of the developed detector blocks were also measured for various SiPM array sizes (4×4 , 8×8 , and 12×12). All energy and timing resolutions were calculated in the full width at half maximum

(FWHM) from a Gaussian fit. None of timing corrections was applied.

3. Results

3.1. Determination of optimal bias voltages

To find the breakdown voltages, energy spectra were obtained under various bias voltages with 0.2 V steps for all 144 SiPMs (Fig. 4(a)). The photo-peak position was selected in each spectrum and was then plotted against bias voltage for all SiPM channels. All of the plots fitted well with a second order polynomial curve (coefficient of determination; $R^2 > 0.99$). The breakdown voltage was defined as the zero-crossing point of the fitted curve in each plot of photo-peak position versus bias voltage (Fig. 4(b)).

Fig. 4(c) shows the breakdown voltage distribution for a 12×12 SiPM array. The breakdown voltage was uniform across the SiPM channels in every SiPM device. Therefore, the average breakdown voltage for each SiPM device (as shown in top-left corner on each SiPM device in Fig. 4(c)) was used in further experiments to simplify the bias voltage supply scheme.

In one SiPM channel of each device, the coincidence time resolutions were measured at various overvoltage levels with 0.2 V steps under different LED threshold levels (i.e. 1.5%, 3.0%, 4.5%, and 6.0% of the 511 keV energy peak). The overvoltage is the difference between the applied bias and breakdown voltages. Fig. 5 shows the coincidence time resolutions of one SiPM channel from each device as a function of the overvoltage under different LED thresholds. The same overvoltage range, from 1.8 to 2.4 V, yielded stable and good coincidence time resolution values for all LED threshold levels. Therefore, a 2.2 V overvoltage was supplied to each SiPM device and a LED threshold level of $\sim 3\%$ was applied to each of the timing measurement signal lines.

3.2. Coincidence time resolution and energy resolution for various SiPM array sizes

To evaluate the proposed method, the coincidence time resolution values were measured using various SiPM array sizes (4×4 ,

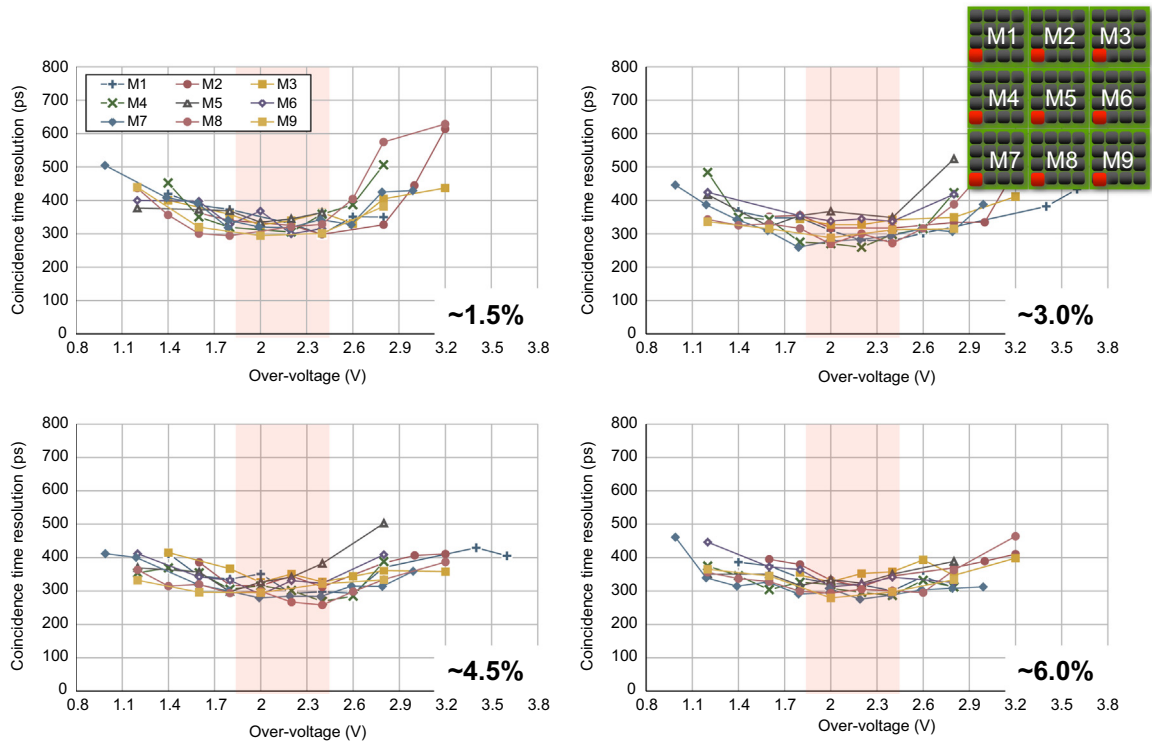


Fig. 5. Coincidence time resolution for one SiPM channel from each device as a function of overvoltage under different LED thresholds (from ~1.5% to 6.0%).

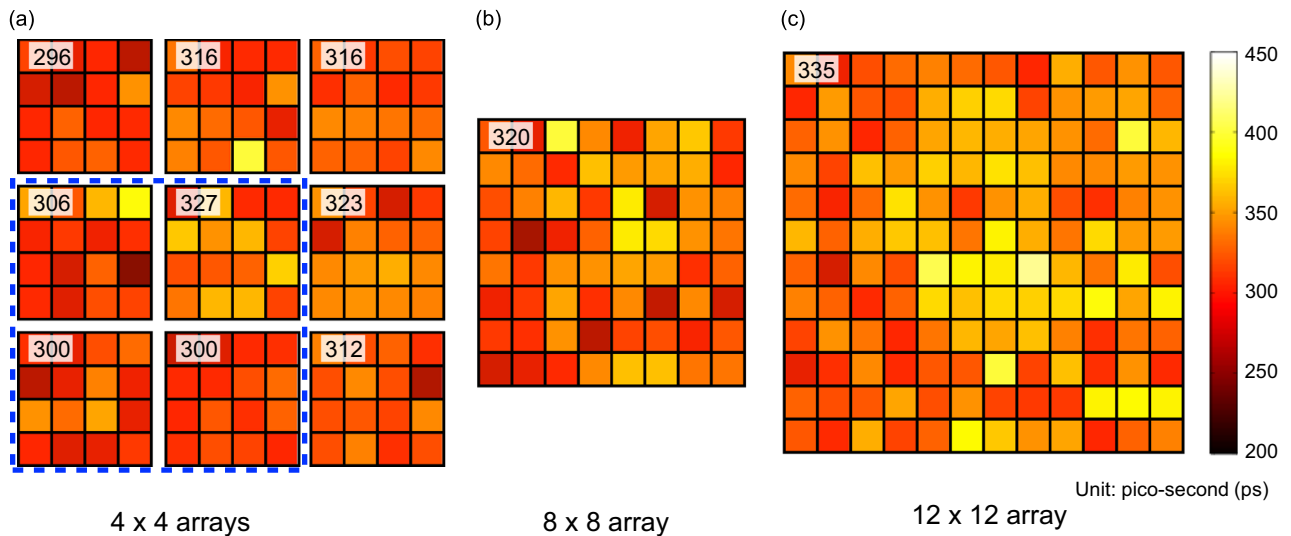


Fig. 6. Distribution of the coincidence time resolutions of nine 4×4 SiPM arrays (a), an 8×8 SiPM array (b), and a 12×12 SiPM array (c). The average coincidence time resolutions of all crystals were 311 ps, 320 ps, and 335 ps, respectively. The blue dashed box indicates the SiPM devices used in the 8×8 SiPM array. (For interpretation of the references to color in this figure legend, the reader is referred to the web version of this article.)

8×8 , and 12×12). These SiPM arrays consist of 1, 4 (2×2), and 9 (3×3) SiPM devices. While all nine SiPM devices were assembled together on the test circuit board, SiPM devices that were not used for the evaluation of smaller array sizes were turned off during these measurements. A reference detector, which consists of R9800 PMT and a $4 \times 4 \times 10 \text{ mm}^3$ LYSO crystal, was used to acquire coincident events and to calculate coincidence time resolutions from a ^{22}Na point source.

Fig. 6(a) shows the coincidence time resolution distribution for all of the 4×4 SiPM arrays. Each average coincidence time resolution of 16 SiPM channels in each 4×4 SiPM array was calculated (MAX: 327 ps, MIN: 296 ps, mean: 311 ps) and noted on

the top-left corner in Fig. 6(a). Four SiPM devices (index numbers: 4, 5, 7, 8 [dashed box in Fig. 6(a)]) were selected to assemble 8×8 SiPM array. Fig. 6(b) and (c) shows the coincidence time resolution distributions of the 8×8 and 12×12 SiPM arrays, respectively. The average resolutions were 320 ± 31 ps (8×8 array) and 335 ± 28 ps (12×12 array). Table 1 shows the single time resolution of SiPM detectors which were calculated by the convolution-subtraction of the single time resolution of reference detector (200 ps), and the expected coincidence time resolutions of two identical SiPM detectors with same array size [11].

The energy resolutions of the various SiPM array sizes were also measured. Fig. 7 shows the energy resolution distributions of

the 4×4 , 8×8 , and 12×12 SiPM arrays. The average energy resolutions of all single SiPM channels in each array were 11.8%, 12.5%, and 12.8%.

3.3. Propagation delay

In this detector array, the column and row signals were projected into a single side. Therefore, there is a difference in the electric signal transmission path lengths, which run from the output pin of each SiPM to the input pin of each amplifier. The path length difference among the SiPM channels resulted in a propagation delay (a trigger time difference relative to the closest channel to the amplifier). Fig. 8 shows the propagation delay among the SiPM channels located along the 4th column of a typical SiPM device (where channel number 13 was the closest channel). From the slope of the plot in Fig. 8, we were able to calculate a constant propagation delay of ~ 111 ps per SiPM channel, which would be useful information when compensating for the related TOF estimation error.

4. Discussion

In this study, we evaluated a projection-based signal encoding method for SiPM arrays in which the row and column projection signals were amplified with different gains to estimate the energy and timing information. Dedicated front-end electronics were developed and the optimal bias voltage for each SiPM was determined by considering stability in the timing resolution. For SiPM arrays with different array sizes, the timing and energy resolutions were compared. The largest array size tested in this

study was 12×12 , and this detector block was $\sim 5 \times 5$ cm² in size, which is equivalent to the size of a block detector using 2×2 one-inch PMTs.

Most properties (i.e. the amplification gain and the dark count rate) of the SiPM output are sensitive to the bias voltage applied to the SiPM. In particular, the SiPM gain increases with increasing overvoltage. A similar gain dependence on bias voltage has also been reported for SiPM devices other than the MPPC used in this study [27,28]. In addition, the change in gain of the SiPM caused by a fractional bias change is much larger than that of the PMT. It is also known that the breakdown voltage and the bias voltage that yields the same amplification gain vary considerably across the devices [12]. Our results (Fig. 4(c)) also show that the breakdown voltage distribution across the devices is not uniform (maximum difference ~ 2 V) because of the lot-to-lot variability in SiPM fabrication. In contrast, the variation of the breakdown voltage across the channels within a device was relatively small, mainly because the multi-channel MPPC S11064-050P used in this study was produced by tiling of discrete single element MPPCs which all had similar responses. Therefore, all 16 channels in a MPPC device could be biased using a single voltage source.

In this study, it was confirmed that the SiPM coupled to a LGSO scintillation crystal produces excellent timing resolution, as shown in Fig. 5. Higher overvoltage values for the SiPM lead to improved photon-detection efficiency (PDE), and improved PDE in turn results in better timing performance because of the improved photoelectron statistics at the rising edge of the output pulse [13,20]. However, overvoltages higher than 2.4 V led to degradation of the timing resolution caused by an increased dark count rate, yielding the typical “U-shaped” relationship between the

Table 1

Measured average coincidence time resolution between SiPM detectors and a reference PMT detector, and calculated single and coincidence time resolutions of SiPM detectors. Single time resolution of the reference PMT detector was 200 ps.

| SiPM array size | Coincidence time resolution (ps) SiPM–PMT | Single time resolution (ps) SiPM | Coincidence time resolution (ps) SiPM–SiPM |
|-----------------|---|----------------------------------|--|
| 4×4 | 316 | 245 | 346 |
| 8×8 | 320 | 250 | 353 |
| 12×12 | 335 | 269 | 380 |

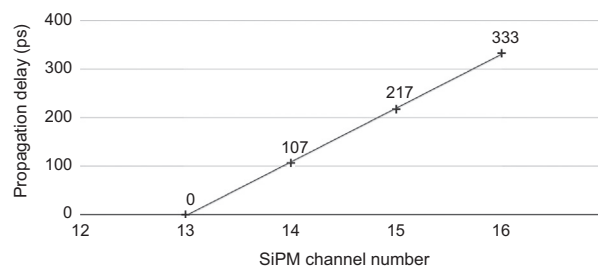


Fig. 8. Propagation delay along the SiPM channels in a typical SiPM device. The SiPM channel number 13 was the closest channel to the input pin of the amplifier.

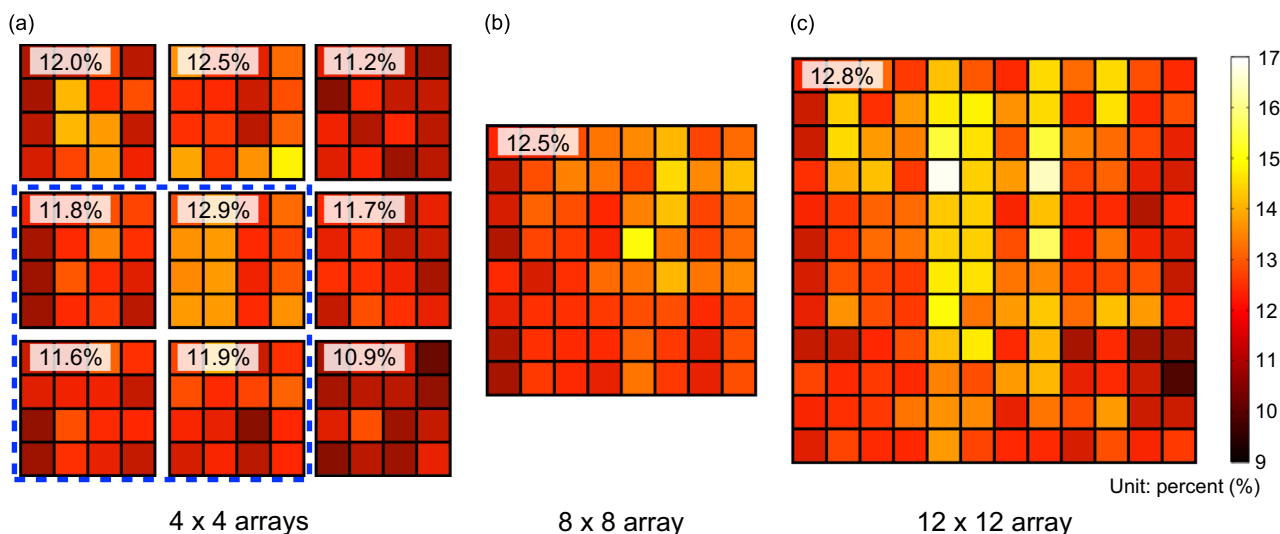


Fig. 7. Distribution of the energy resolutions of nine 4×4 SiPM arrays (a), an 8×8 SiPM array (b), and a 12×12 SiPM array (c). The average energy resolutions of all crystals were 11.8%, 12.5%, and 12.8%, respectively. The blue dashed box indicates the SiPM devices used in the 8×8 SiPM array. (For interpretation of the references to color in this figure legend, the reader is referred to the web version of this article.)

coincidence timing resolution and the overvoltage shown in Fig. 5. Regardless of their LED thresholds, all tested MPPCs yielded this common “U-shape” relationship, with the flat region of minimal coincidence timing resolution at an overvoltage of around 2.2 V. Fig. 5 also shows that the coincidence timing resolution is best when a 3.0% LED threshold was applied. The lower threshold is able to trigger early detection of photons, but is vulnerable to electronic noise.

The coincidence time and energy resolutions of the detector modules with the various SiPM array sizes (4×4 , 8×8 , and 12×12) were measured with a 2.2 V overvoltage and a $\sim 3\%$ LED threshold level. Detector modules containing the 4×4 array yielded consistent and good timing and energy resolution values.

As the SiPM array size increased, the average coincidence time resolution also increased. This was mainly because of the increasing number of connected column-side SiPM channels, which were used to measure the timing information. This leads to greater dark count noise for each column output in the current readout scheme. Increased count rates due to the intrinsic lutetium radioactivity of the LGSO crystal would also affect the coincidence time resolution. SiPM output pulses caused by both dark count noise and intrinsic activity have long tails [20], leading to a higher frequency of pulse pileup and baseline shift, which both have adverse effects on the timing resolution. The baseline shift is also enlarged by the other connected SiPM channels. However, the difference in coincidence timing resolution between the 4×4 and 12×12 arrays was only 24 ps. Results from 4×4 SiPM array were comparable with previous work that used a similar SiPM device and measured coincidence time resolutions without any signal encoding scheme [22]. The energy resolution also increased slightly as the SiPM array size increased. However, this difference was also negligible. From these results, the proposed concept can be used in cost effective PET block detectors for human PET scanner with minimal degradation of time performance.

The implemented circuit in this study used only an anode output of each SiPM channel. But the proposed concept can adopt any possible alternative encoding schemes, which can be split into rows and columns. If a different kind of SiPM [29] which has three outputs (cathode, anode, and fast output) is used, the circuit will be more simplified. Moreover, time performance will also be able to be improved since a fast output of each SiPM will be used for column connections in the proposed concept.

The system performance of the PET is determined by several factors, including the spatial, timing, and energy resolutions, and the sensitivity. The crystal block used in this study does not have a sufficiently high packing fraction to yield the best gamma ray detection efficiency because we used pixelated LGSO crystals with the same front surface area ($3 \times 3 \text{ mm}^2$) as the sensitive area of each SiPM. We matched these sizes to collect as much of the scintillation light as possible. The effects of the size mismatch (a larger crystal size than the SiPM sensitive area) will be addressed in further studies, although the packing fraction of the SiPM is also improving (49.4% in the MPPC array used in this study, but up to 74.0% in the latest version of the MPPC array).

5. Conclusion

A signal encoding method for a TOF PET block detector using SiPMs to reduce the complexity and volume of the signal readout and processing electronics required has been validated. The proposed method showed promising results, which were measured for various SiPM array sizes.

Acknowledgments

This work was supported by grants from the Atomic Energy R&D Program (Grant nos. 2008-2003852 and 2010-0026012) and the WCU Program (Grant no. R32-10142) through the KOSEF, which is funded by the Korean Ministry of Education, Science and Technology.

References

- [1] B.J. Pichler, H.F. Wehrli, M.S. Judenhofer, *Journal of Nuclear Medicine* 49 (2008) 55.
- [2] J.S. Lee, *Open Nuclear Medicine Journal* 2 (2010) 192.
- [3] W.W. Moses, *IEEE Transactions on Nuclear Science* NS50 (2003) 1325.
- [4] J.S. Karp, S. Surti, M.E. Daube-Witherspoon, G. Muehllehner, *Journal of Nuclear Medicine* 49 (2008) 462.
- [5] M. Conti, *Physica Medica-European Journal of Medical Physics* 25 (2009) 1.
- [6] J.S. Karp, G. Shakirin, F. Fiedler, W. Enghardt, A. Wagner, *Physics in Medicine and Biology* 52 (2007) 6795.
- [7] S. Vandenberghe, I. Lemahieu, *Nuclear Instruments and Methods in Physics Research Section A* 571 (2007) 480.
- [8] S. Surti, J.S. Karp, *Physics in Medicine and Biology* 53 (2008) 2911.
- [9] T. Moriya, T. Omura, M. Watanabe, T. Yamashita, *IEEE Transactions on Nuclear Science* NS55 (2008) 2455.
- [10] J.P. Lee, M. Ito, J.S. Lee, *Biomedical Engineering Letters* 1 (2011) 174.
- [11] M. Ito, J.P. Lee, J.S. Lee, *IEEE Transactions on Nuclear Science* NS60 (2013) 30.
- [12] J.S. Lee, S.J. Hong, *Geiger-mode avalanche photodiodes for PET/MRI, Electronic Circuits for Radiation Detection*, CRC Press, Boca Raton (2010) 179.
- [13] E. Roncali, S.R. Cherry, *Annals of Biomedical Engineering* 39 (2011) 1358.
- [14] A. Kolb, et al., *Physics in Medicine and Biology* 55 (2010) 1815.
- [15] S. Yamamoto, et al., *Physics in Medicine and Biology* 55 (2010) 5817.
- [16] S.I. Kwon, et al., *Journal of Nuclear Medicine* 52 (2011) 572.
- [17] S.J. Hong, et al., *Physics in Medicine and Biology* 57 (2012) 3869.
- [18] H.S. Yoon, et al., *Journal of Nuclear Medicine* 53 (2012) 608.
- [19] G.B. Ko, et al., *Nuclear Instruments and Methods in Physics Research Section A* 703 (2013) 38.
- [20] C.L. Kim, G.C. Wang, S. Dolinsky, *IEEE Transactions on Nuclear Science* NS56 (2009) 2580.
- [21] D.R. Schaart, et al., *Physics in Medicine and Biology* 55 (2010) 179.
- [22] C.L. Kim, D.L. McDaniel, A. Ganin, P.E.T. Time-of-flight, *IEEE Transactions on Nuclear Science* NS58 (2011) 3.
- [23] V. Popov, S. Majewski, A.G. Weisenberger, *IEEE Nuclear Science Symposium Conference Record* 3 (2003) 2156.
- [24] S. Yamamoto, H. Watabe, J. Hatazawa, *Physics in Medicine and Biology* 56 (2011) 227.
- [25] S.J. Hong, et al., *IEEE Transactions on Nuclear Science* NS55 (2008) 912.
- [26] S. Shimizu, et al., *IEEE Transactions on Nuclear Science* NS53 (2006) 14.
- [27] Y. Musienko, S. Reucroft, J. Swain, Tests and performance of multi-pixel Geiger mode APD's, in: *Proceedings of the International Workshop on New Photon-detectors*, Kobe, Japan, 2007.
- [28] M. Ramilli, Characterization of SiPM: temperature dependencies, in: *Proceedings of the IEEE Nuclear Science Symposium Conference Record*, 2008, p. 2467.
- [29] J.-Y. Yeom, et al., Performance of fast timing silicon photomultipliers for scintillation detectors, in: *Proceedings of the IEEE Nuclear Science Symposium Conference Record*, 2012, p. 2845.